Research Article

Cancer Immunology Research

Tumor Cells Hijack Macrophage-Produced Complement C1q to Promote Tumor Growth

Lubka T. Roumenina[1,2,3], Marie V. Daugan[1,2,3], Rémi Noé[1,2,3], Florent Petitprez[2,3,4,5], Yann A. Vano[2,3,4,6], Rafaël Sanchez-Salas[7], Etienne Becht[2,3,4], Julie Meilleroux[1,2,4,8], Bénédicte Le Clec'h[1,2,4], Nicolas A. Giraldo[2,3,4], Nicolas S. Merle[1,2,3], Cheng-Ming Sun[2,3,4], Virginie Verkarre[2,9], Pierre Validire[10], Janick Selves[8], Laetitia Lacroix[2,3,4], Olivier Delfour[11], Isabelle Vandenberghe[11], Celine Thuilliez[11], Sonia Keddani[1,2,3], Imene B. Sakhi[1,3], Eric Barret[7], Pierre Ferré[11], Nathalie Corvaïa[11], Alexandre Passioukov[11], Eric Chetaille[11], Marina Botto[12], Aurélien de Reynies[5], Stephane Marie Oudard[6], Arnaud Mejean[2,13], Xavier Cathelineau[2,7], Catherine Sautès-Fridman[2,3,4], and Wolf H. Fridman[2,3,4]

Abstract

Clear-cell renal cell carcinoma (ccRCC) possesses an unmet medical need, particularly at the metastatic stage, when surgery is ineffective. Complement is a key factor in tissue inflammation, favoring cancer progression through the production of complement component 5a (C5a). However, the activation pathways that generate C5a in tumors remain obscure. By data mining, we identified ccRCC as a cancer type expressing concomitantly high expression of the components that are part of the classical complement pathway. To understand how the complement cascade is activated in ccRCC and impacts patients' clinical outcome, primary tumors from three patient cohorts ($n = 106$, 154, and 43), ccRCC cell lines, and tumor models in complement-deficient mice were used. High densities of cells producing classical complement pathway components C1q and C4 and the presence of C4 activation fragment deposits in primary tumors correlated with poor prognosis. The *in situ* orchestrated production of C1q by tumor-associated macrophages (TAM) and C1r, C1s, C4, and C3 by tumor cells associated with IgG deposits, led to C1 complex assembly, and complement activation. Accordingly, mice deficient in C1q, C4, or C3 displayed decreased tumor growth. However, the ccRCC tumors infiltrated with high densities of C1q-producing TAMs exhibited an immunosuppressed microenvironment, characterized by high expression of immune checkpoints (i.e., PD-1, Lag-3, PD-L1, and PD-L2). Our data have identified the classical complement pathway as a key inflammatory mechanism activated by the cooperation between tumor cells and TAMs, favoring cancer progression, and highlight potential therapeutic targets to restore an efficient immune reaction to cancer.

Introduction

Renal cell cancer (RCC) is the cause of over 140,000 deaths per year (1). RCC encompasses different histologic subtypes, with clear-cell RCC (ccRCC) representing 75% of the cases. ccRCC is still a clinical challenge, particularly at the metastatic stage when surgery has limited efficacy. In addition to high vascularization (due, in part, to the Von Hippel-Lindau, VHL mutations), many ccRCC tumors have an immune and inflammatory cell infiltrate. These tumors display a disorganized tumor microenvironment (TME), where a high density of $CD8^+$ T cells, showing an exhausted phenotype, correlates with shorter survival (2). Tumor-associated macrophages (TAM) exhibit M2-like functions,

[1]INSERM, UMR_S 1138, Cordeliers Research Center, Team "Complement and diseases", Paris, France. [2]Sorbonne Paris Cite, Cordeliers Research Center, University Paris Descartes Paris 5, Paris, France. [3]Cordeliers Research Center, Sorbonne University, Paris, France. [4]INSERM, UMR_S 1138, Cordeliers Research Center, Team "Cancer, Immune Control and Escape", Paris, France. [5]Programme Cartes d'Identité des Tumeurs, Ligue Nationale contre le Cancer, Paris, France. [6]Department of Oncology, Georges Pompidou European Hospital, Assistance Publique Hopitaux de Paris, Paris, France. [7]Department of Urology, Institut Mutualiste Montsouris, Paris, France. [8]Department of Pathology, Institut Universitaire du Cancer Toulouse – Oncopole, Toulouse, France. [9]Department of Pathology, Georges Pompidou European Hospital, Assistance Publique Hopitaux de Paris, Paris, France. [10]Department of Pathology, Institut Mutualiste Montsouris, Paris, France. [11]Pierre Fabre Research Institute, Toulouse, France. [12]Department of Medicine, Imperial College London, London, United Kingdom. [13]Department of Urology, Georges Pompidou European Hospital, Assistance Publique Hopitaux de Paris, Paris, France.

Note: Supplementary data for this article are available at Cancer Immunology Research Online (http://cancerimmunolres.aacrjournals.org/).

Current address for E. Becht: Singapore Immunology Network (SIgN), Agency for Science, Technology and Research (A*STAR), Singapore; and current address for N. A. Giraldo, Pathology Department, Johns Hopkins Hospital, Baltimore, Maryland.

L.T. Roumenina, M.V. Daugan, and R. Noé contributed equally to this article.

Corresponding Authors: Lubka T. Roumenina, Cordeliers Research Center, INSERM UMRS 1138, 15 rue de l'Ecole de Medecine, Escalier E, Paris 75006, France. Phone: 3301-4427-9087; Fax: 331-4051-0420; E-mail: lubka.roumenina@crc.jussieu.fr; and Wolf H. Fridman, herve.fridman@crc.jussieu.fr

Cancer Immunol Res 2019;7:1091–105

doi: 10.1158/2326-6066.CIR-18-0891

favoring cancer growth, neovascularization, and invasion (3–5). In fact, in-depth immune profiling reveals that TAMs represent a heterogeneous cell population in ccRCC tumors, with one population, annotated M5, being associated with T-cell exhaustion (6). Understanding how local inflammation modulates T-cell function and impacts patients' prognosis are indispensable to define novel targets for immunotherapy to restore an efficient immune reaction in ccRCC (7–9).

The complement system is one of the key factors in tissue inflammation (10), and animal models demonstrate that complement component 5a (C5a), generated within the TME, promotes cancer progression by activating angiogenesis and driving immunosuppression (11–13). C5a production can be generated through: (i) the classical pathway starting with C1 activation, (ii) the alternative pathway starting with direct activation of C3, or (iii) the lectin pathway (13). A study has also demonstrated that C5a can be generated in a cascade-independent manner in a mouse model of squamous carcinogenesis (14).

Kidneys produce a large spectrum of complement proteins allowing *in situ* cascade activation, leading to a variety of inflammatory diseases due to complement activation or dysregulation (14–16). Therefore, we investigated the mechanisms of complement cascade activation in ccRCC tumors and their consequences on the TME and patients' prognosis. Our data show that tumor cells produce C1r, C1s, C4, and C3 *in situ*, and C1r and C1s highjack TAM-produced C1q for *in situ* formation of the initiating C1 complex and activation of the classical pathway on intratumoral immune complexes. The expression of C1q and the density of the $C1q^+$ TAM subset correlated with an exhausted T-cell phenotype and poor clinical outcome. The production of C4 and C3, as well as the deposition of C4 fragments, was also associated with poor prognosis. Collectively, our data provide evidence for activation of the classical pathway in ccRCC by cooperation between tumor cells and TAMs, causing immune modulation and increasing the risk of cancer progression.

Materials and Methods

Transcriptomic analyses

The gene expression for *C1QA*, *C1QB*, *C1QC*, *C1R*, *C1S*, *C2*, *C3*, *C4*, and *C3AR1* were assessed using the average Fragments Per Kilobase Million (FPKM) values from Human Protein Atlas in 20 different cancer cohorts available (17). Liver cancer was excluded from the analyses, because the liver tissue is the major production site for complement. The heatmap is generated using R software 3.4.2 with heatmap.2 package. The correlation between the *C1QA* gene and the endothelial cell gene signature was evaluated in the transcriptomic data of The Cancer Genome Atlas (TCGA) cohort and our Cohort 3 using the Microenvironment Cell Populations-counter (MCP-counter) software as described previously (18). No correlation was found. Normalized RNA-sequencing (RNA-Seq) data were downloaded from the GDC data portal (TCGA-KIRC cohort) and $\log_2$-transformed. The correlations between gene expression were computed using Pearson coefficient and a subsequent non-nullity test using R software version 3.4.2. Processed RNA-Seq data from the study by Chevrier and colleagues (6) were downloaded from ArrayExpress (accession code: E-MTAB-5640). Differential gene expression between M5 and control macrophages was estimated using Mann–Whitney tests with R software version 3.4.2.

Patients

Study approval. All the included patients signed an informed consent form prior to inclusion in the study, and the research was approved by the medical ethics board of all participating institutions (no. CEPAR-2014-001). The study was conducted according to the recommendations in the Helsinki Declaration.

Cohort descriptions. Primary ccRCC tumor specimens were collected from three retrospective cohorts. Inclusion criteria for the study were: histology type ccRCC, all tumor–node–metastasis (TNM) stages (except cohort 3, which included only stage IV). The patients lacking clinical data and slides with poor quality tissue were excluded. Tumor specimens were included in paraffin and stored at 4°C. Slides with 3-μm sections were kept at 4°C until use.

Cohort 1 included 106 patients undergoing nephrectomy at Necker-Enfants Malades Hospital (Paris, France) between 1999 and 2003 (2). Cohort 2 was comprised of 154 patients operated on at the Institut Mutualiste Montsouris (IMM; Paris, France) between 2002 and 2010. Cohort 3 included 43 metastatic patients receiving surgery at one Belgian and three French hospitals from 1994 to 2011 (19). A prospective cohort composed of seven randomly selected patients recruited in 2017 at IMM was also used. Histopathologic features, such as histologic subtype, tumor size, Fuhrman nuclear grade, and TNM stage were available for the majority of the patients (Table 1), and the duration of follow-up was calculated from the date of surgery to the date of cancer progression, last follow-up, or death. A TCGA-KIRC (kidney clear cell carcinoma) cohort composed of 537 primary ccRCC samples with clinical and transcriptomic data was also used in this study. All available data were used, expressed as average FPKM.

IHC and immunofluorescence for complement detection

Human tissues. Formalin-fixed paraffin-embedded (FFPE) human tumor specimens were cut into 3-μm–thick sections and stained for C1q, C4d, C3d, IgG, CD163, LAG3, and PD-1 Supplementary Table S1. Human FFPE tonsil sections were used as a positive control for C1q, C4d, CD163; liver sections as positive controls for C3, C4; and mannan-binding lectin (MBL) and sections from skin of the patients with pemphigus vulgaris (Geneticist) for C3d (Supplementary Fig. S1). For each stain, an isotype control was also used. The specificity of the anti-C1q, anti-C3d, and anti-C4d was verified by a competition test (Supplementary Fig. S1A—S1C).

The antigen retrieval was carried out on a PT-link (Dako) using the EnVision FLEX Target Retrieval Solutions (Dako) with low or high pH for the detection of C1q, C4d, C3d, CD163, LAG3, and PD-1 or with Proteinase K (Dako, S3020) for IgG staining. Endogenous peroxidase and nonspecific staining were blocked with 3% H_2O_2 (Gifrer, 10603051) and protein block (Dako, X0909), respectively. The primary and secondary antibodies used for IHC and IF are summarized in Supplementary Table S3. For IHC studies, staining was revealed with 3-amino-9-ethylcarbazole substrate (Vector Laboratories, SK-4200). After mounting either with glycergel (Dako, C056330-2) for IHC or ProLong Gold antifade reagent with DAPI (Thermo Fisher Scientific, P36935) for IF, the slides were scanned with Nanozoomer (Hamamastu) for IHC or Axio Scan (Zeiss) for IF. Stained slides were analyzed by Calopix software (Tribvn). For CD163, LAG3, and PD-1 markers, the density of positive cells was quantified in the tumor core and in the invasive margin. The percent colocalization between

Table 1. Demographic and clinical characteristics of the analyzed patients in the 4 ccRCC cohorts

ccRCC Retrospective cohort 1		**ccRCC Retrospective cohort 2**		**ccRCC Retrospective cohort 3**		**ccRCC Prospective cohort**	
Number of patients	106	Number of patients	154	Number of patients	43	Number of patients	7
Males, *n* (%)	80 (75%)	Males, *n* (%)	104 (68%)	Males, *n* (%)	31 (74%)	Males, *n* (%)	NA
Age (years)	63	Age (years)	62	Age (years)	56	Age (years)	59
OS time (days)	2,107	OS time (days)	NA	OS time (days)	1,220	OS time (days)	NA
Progression-free survival (days)	2,094	Progression-free survival (days)	1,179	Progression-free survival (days)	877	Progression-free survival (days)	NA
Tumor size major axis (cm)	5.25	Tumor size major axis (cm)	NA	Tumor size major axis (cm)	NA	Tumor size major axis (cm)	NA
Sarcomatoid variant	12 (11%)	Sarcomatoid variant	2 (1%)	Sarcomatoid variant	13 (31%)	Sarcomatoid variant	NA
TNM Stage		TNM Stage		TNM Stage		TNM Stage	
I	42 (40%)	I	61 (40%)	I	0	I	3 (43%)
II	6 (6%)	II	7 (5%)	II	0	II	1 (14%)
III	43 (41%)	III	83 (54%)	III	0	III	2 (29%)
IV	15 (14%)	IV	3 (2%)	IV	43 (100%)	IV	1 (14%)
Fuhrman grade		Fuhrman grade		Fuhrman grade		Fuhrman grade	
I	5 (5%)	I	1 (1%)	I	0 (0%)	I	0 (0%)
II	23 (22%)	II	32 (21%)	II	0 (0%)	II	4 (57%)
III	62 (58%)	III	102 (66%)	III	19 (44%)	III	2 (29%)
IV	15 (14%)	IV	19 (12%)	IV	23 (53%)	IV	1 (14%)
NA	1 (1%)	NA	0 (0%)	NA	1 (2%)	NA	0 (0%)

NOTE: Cohort 1 comprises (in part) patients published in ref. 2 and cohort 3 is published in ref. 19.

different staining patterns revealed by immunofluorescence (IF) was calculated using HALO Image Analysis Software (Indica Labs) in selected sections, rich of C1q-positive infiltrating cells or C1q deposits.

The specificity of the anti-C1q and anti-C4d antibodies was verified by a competition test as follows: for the anti-C1q antibodies, the primary antibodies were incubated with human C1q (Comptech, A099) or C3b (Comptech, A114); for C4d, the primary antibody was preincubated with recombinant human C4d (Abcam, ab 198640) or purified human C3d (Comptech, A112); for C3d, the primary antibody was preincubated with purified human C3d (Comptech, A112) or purified human C1r (Comptech, A102). The incubation was performed for 1 hour at different molar ratios (0:1, 1:1, and 1:2). The staining of the tonsil sections was inhibited after preincubation of the antibody with purified C1q, C4d, or C3d, respectively, but not with purified C3b, C3d, or C1r.

For the C4a/C4d and C1q/C4d double staining, a tyramide system was used. The incubation with AF647 tyramide reagent (1:100 diluted in TBS 1×, H_2O 0.0015%, Life Technologies, B40958) was performed after the secondary horseradish peroxidase (HRP)-coupled antibody and was followed by antibody stripping at 97°C for 10 minutes. This protocol was repeated for the second primary and secondary antibody incubations and AF546 tyramide reagent diluted 1/100 (B40954).

The detection of mRNA expression of C1r and C1s *in situ* in ccRCC tumors was performed by RNAscope technology (ACDbio) using the manufacturer's instructions.

Classification method for C1q, C4 and C3 staining in ccRCC tumors

C1q staining classification. Tumors were scored into three groups according to the percentage of C1q-producing cells within the tumor (at any intensity). This semiquantification was performed by three independent observers as follows: score 0 (weak): cutoff <1% of nonneoplastic cells; 1 (intermediate): 1–30% of nonneoplastic cells; 2 (strong): >30% of nonneoplastic cells. Patients with score 2 staining were found to have a shorter survival than any other score for both progression-free survival (PFS) and overall survival (OS; $P = 0.0216$ and $P = 0.0165$, respectively). Therefore, all subsequent studies were performed separating tumors into C1q high (score 2) and C1q low (scores 0 to 1) staining. An automated quantification of the immune-reactive area for C1q for the whole slide scans of cohort 3 was performed using HALO Image Analysis Software (Indica Labs). The training of the algorithm to distinguish between infiltrating cells, vessels, and deposits did not result in reliable distinction between the patterns. Therefore, we retained the semiquantification as a method for analysis for this study.

C4/C3 staining classification. Tumors were classified into three staining scores according to the percentage of C4/C3 cytoplasmic staining in tumor cells or C4d/C3d deposits on the membrane of tumor cells (at any intensity). The semiquantification was performed by three independent observers as follows: score 0 (weak): cutoff <1% of nonneoplastic cells; 1 (intermediate): 1–30% of nonneoplastic cells; 2 (strong): >30% of nonneoplastic cells.

The density of C4-producing tumor cells showed a trend toward association with shorter PFS ($P = 0.09$) and a significant association with OS ($P = 0.04$). Because the survival curves overlapped for scores 1 and 2 tumors, these tumors were pooled into a high group.

We found a significant negative impact of C4 activation fragment deposits on PFS ($P = 0.04$) and a trend for the OS ($P = 0.08$) in tumors of patients with staining score 2. Because the survival curves of staining scores 0 and 1 tumors were indistinguishable, these tumors were pooled into a low group.

RNAscope

FFPE human tumor specimens were cut into 3-μm–thick sections. The detection of mRNA expression of C1r and C1s *in situ* in ccRCC tumors was performed by RNAscope technology using the kit ACDbio universal VS sample Prep Reagents (323220). Negative control probe (ACDbio, 312039), positive control probe (ACDbio, 313909), and probe targeting either human C1s (ACDbio, 508969) or human C1r (ACDbio, 508959) were used.

Cell lines and culture conditions

The human ccRCC cell lines Caki-1 and A498, as well as control cell lines from colorectal cancer (HCT116 and SW620), were purchased from the ATCC. Caki-1 and HCT116 cells were cultured in McCoy's medium (Gibco) + 10% FCS + 1× penicillin/streptomycin (Gibco). SW620 cells were cultured in Leibovitz medium (Gibco) + 10% FCS 1× penicillin/streptomycin (Gibco), and A498 cells were cultured in Eagle minimum essential medium (ATCC) + 10% FCS + 1× penicillin/streptomycin (Gibco) in a humidified atmosphere of 5% CO_2 and 95% air at 37°C. The cells were cultured until approximately 70% confluence and the culture medium was changed to reduced serum medium Opti-MEM (Thermo Fisher Scientific). The supernatant was recovered 48 hours later.

Mouse TC-1, MC38, B16F0 melanoma, LLC lung adenocarcinoma, and MCA205 fibrosarcoma cell lines were tested *in vitro*. The cells were cultured in RPMI supplemented with 5 mmol/L glutamine (Gibco), 10% FCS, 1× penicillin/streptomycin (Gibco), and 50 μmol/L 2-mercaptoethanol (Gibco). No specific authentication of the cell lines was performed. They were routinely tested for *Mycoplasma* and used when negative.

Western blot analysis for complement

After 48 hours of culture in a synthetic medium without serum, the supernatants of the human and mouse cell lines were recovered and concentrated using Amicon Ultracel 3K units (UFC 900324). The samples were prepared with NuPAGE LDS sample buffer (4×; Thermo Fisher Scientific) with or without reducing agent (DTT) and then denatured at 80°C for 10 minutes. Proteins were separated in NuPAGE 10% Bis-Tris gel (Thermo Fisher Scientific). The proteins were transferred onto a nitrocellulose membrane using iBlot (Invitrogen). The membranes were then stained with the SNAP i.d. Protein Detection System (Millipore) using a primary goat anti-human C1s antiserum (Quidel, A302; 1/5000), polyclonal rabbit anti-human C1r (Abcam, ab155060, 1/500), rabbit polyclonal anti-mouse C1r (Abcam ab205546, 1/500), rabbit polyclonal anti-mouse C1s (Abcam ab199418, 1/500), rabbit polyclonal anti-human C4 (Siemens, OSAO, 1/500), and goat polyclonal anti-human C3 (Merck Millipore 204869, 1/5,000). Secondary antibodies were rabbit anti-goat HRP (Santa Cruz Biotechnology H0712, 1/10,000) or a goat anti-rabbit HRP (Santa Cruz Biotechnology J512, 1/5,000). After washes, the membranes were developed with an ECL Reagent (Pierce #32106), and the chemiluminescence was detected with a MyECL Imager (Thermo Fisher Scientific). The purified human proteins C1s (CompTech, A104) or C1r (CompTech, A102) or mouse serum were used as positive controls.

Functional assays for C1 complex formation and activity

C1 complex formation. To test the formation of a C1 complex, an ELISA was used, as described previously (20). A polyclonal rabbit anti-human C1q (Dako, A0136; diluted 1/1,000 in PBS), was coated overnight on 96-well Nunc plates (Nunc MaxiSorp). A 1% BSA solution was then used for blocking for 1 hour at room temperature. The washing steps were performed with TBS Tween with 0.05% $CaCl_2$ (1 mmol/L). The supernatants of cultured human cell lines, supplemented with increasing doses of human C1q (Comptech, A099, from 0.125 to 2 μg/mL diluted in washing buffer) were added to the plates and incubated for 1 hour at 37°C. Increasing doses of normal human serum were added as positive controls. A goat anti-human C1s antiserum (Quidel, A302; 1/500 diluted in the washing buffer) was used and incubated for 1 hour at 37°C, and a secondary rabbit anti-goat HRP (1/2,000 diluted for human; Santa Cruz Biotechnology, H0712) was then added. The ELISA was revealed with SureBlue TMB Microwell Peroxidase Substrate (KPL), and the reaction was stopped with 2 mol/L sulfuric acid. The optical density at 450 nm was measured by Multiskan Ex (Thermo Fisher Scientific).

Functional activity of C1. To evaluate the functionality of this C1 complex, another ELISA-based functional test was set up as in ref. 21. The 96-well plates were coated with human IgG1 (50 μg/mL) for 1 hour at 37°C. A solution of 1% BSA was then used to block the plate for 1 hour at room temperature. The washing steps were performed with 10 mmol/L HEPES, 75 mmol/L NaCl, 1 mmol/L $CaCl_2$, 1 mmol/L MgCl, and 0.05% Tween 20. The supernatants of cultured cell lines and increasing doses of human C1q (from 0.125 to 4 μg/mL, diluted in washing buffer) were added to the plates and incubated for 1 hour at 37°C. In the same plate, increasing doses of human serum (diluted from 1/1,280 to 1/40) were added as a positive control. A solution containing human C4 protein (4 μg/mL; Comptech, A105) and C2 protein (5 μg/mL; Comptech, A112) were then added and incubated for 2 hours and 30 minutes at 37°C. The supernatant from the wells was recovered, and the C2 cleavage was analyzed by Western blotting under reducing conditions using biotinylated antihuman C2 (R&D Systems, BAF1936; diluted 1/400) and then streptavidin HRP (1/3,000; Dako, P0397). The signal was revealed as above. The C4 fragment deposits on the plate were detected using an anti-C4 antibody (Siemens, OSAO; diluted 1/500) and a secondary rabbit anti-goat HRP (Santa Cruz Biotechnology, H0712; diluted 1/2,000).

Interaction of tumor cells with C1q *in vitro*

The interaction of two human ccRCC cells lines (Caki-1 and A498), as well as of the mouse cancer cell line TC-1 with immobilized C1q was studied by IF. SuperFrost Plus slides were divided by Dakopen into four equivalent parts, coated either by BSA (Sigma), human C1q (CompTech, A099), or fibronectin (Sigma, F1141) at 20 μg/mL; 2×10^5 cells/quadrant, suspended in Opti MEM (Gibco, 31985-062) medium were placed in each part. After an overnight incubation at 37°C, the cells on the slides were washed and fixed with 4% paraformaldehyde (PFA) for 30 minutes. After an antigen retrieval at low pH and blocking with protein block (Dako, X0909), goat anti-mouse antibody Na/K ATPase followed by anti-mouse IgG-Cy3 was used. After nuclear staining with DAPI and mounting with ProLong Gold antifade reagent (Thermo Fisher Scientific, P36934), the slides were scanned using AxioScan (Zeiss). The nuclei were counted using Visiopharm software. Alternatively, adhesion on these surfaces was evaluated at 5, 10, and 30 minutes after seeding. Proliferation of the tumor cells in the presence of human C1q, albumin, or buffer was evaluated using staining with CFSE CellTrace (CFSE Cell Proliferation Kit Protocol, Thermo Fisher Scientific).

Macrophage sorting

After tissue dissociation, fresh human tumors were incubated for 1 hour at 4°C with 15 mL of Cell Recovery Solution (Thermo Fisher Scientific). Immune populations were separated using Ficoll-Paque PLUS (GE Healthcare Life Science). Cells were then stained with CD14-APC, CD16–APC-H7, CD3-PE, CD66b-PE,

CD19-PE, CD56-PE, and DAPI for viability (Supplementary Table S2). $CD14^+$ cells were sorted using a FACS Cell Sorter BD Aria III with a purity over 95%. These macrophages were recovered in RLT reagent (Qiagen, 79216)-β-mercaptoethanol solution and stored at −80°C.

qRT-PCR

The RNA was extracted from TAMs sorted from the tumors of seven consecutive patients with ccRCC and from mouse and human tumor cell lines or mouse tumors using an RNAeasy Micro Kit (Qiagen, 74004). The quality and quantity of RNA were determined with a 2100 Bioanalyzer (Agilent) using an Agilent RNA 6000 Pico Assay Kit (5067–1513) or Nano Assay Kit (5067–1511). The reverse transcription was performed with 250 ng RNA with the Applied Biosystems High-capacity cDNA Reverse Transcription Kit (Applied Biosystems, 4368814) for the cell lines and mouse tumors. For the mRNA extracted from TAMs, reverse transcription and preamplification were conducted with the Ovation Pico Kit (Nugen, 3302). The quantitative gene expression was assessed by using custom low-density array plates with a TaqMan 7900HT Fast Real-Time PCR System (Applied Biosystems). Expression levels were determined using threshold cycle (C_t) values normalized to *GAPDH* (ΔC_t) and expressed with $2–\Delta C_t$. The references of the primers used for human and mouse gene expression are given in Supplementary Tables S3 and S4, respectively. The RNA was also extracted from mouse tumors and the expression of *Vegfc* (Mm00437310_m1) was assessed. Actin served as an endogenous control (Mm00607939).

Mouse models

Study approval. C57BL/6J mice were purchased from Charles River Laboratories. $C1q^{-/-}$ mice, generated and provided by Prof. Marina Botto (Imperial College London, London, UK) were bred in our animal facility as described previously (22, 23). $C3^{-/-}$ and $C4^{-/-}$ mice were from The Jackson Laboratory. Complement-deficient mice were backcrossed in-house for four generations. Male and female 8 to 10 week-old $C1q^{-/-}$, $C4^{-/-}$, and $C3^{-/-}$ mice and paired groups of wild-type (WT) mice were used in this study. All experiments were conducted in accordance with the recommendations for the care and use of laboratory animals and with approvals APAFIS#34\0-2016052518485390v2 and #9853–2017050211531651v5 by the French Ministry of Agriculture.

Experimental procedure. The mouse TC-1 lung epithelial cell line (transformed by human papillomavirus; ref. 24) was used for *in vivo* experiments. The cells were cultured during one week in complete medium. After 2 to 3 passages, cells were recovered at 80% confluence, and 4×10^5 cells were inoculated subcutaneously (s.c.) in the right flank with 200 μL PBS. Tumor size was measured with calipers every 2 to 3 days for 25 days or until reaching the ethical endpoint of tumor size approaching 3,000 mm^3. Tumors were recovered and were either frozen in liquid nitrogen for IF staining and gene expression analyses or used fresh for flow cytometry analyses.

Flow cytometry on mouse tumors. Intracellular staining for C1q in mouse tumors: freshly recovered mouse tumor tissues were dissociated with enzymatic solution: collagenase I (Thermo Fisher Scientific catalog no. 17100-017, 200 U/mL) and DNase I (Thermo Fisher Scientific catalog no. 90083, 10 U/mL), and then mechanically dissociated by using gentleMACS (Miltenyi Biotec). The solutions were filtered with 70- and 30-μm nylon membrane filters and washed with PBE (PBS, 0.5% BSA, 2 mmol/L EDTA) to obtain single-cell suspensions. The total number of cells was counted using Kovas slides. Two million live cells were distributed in V-shaped 96-well plates and were incubated with Fc Block (anti-CD16/CD32, BD Biosciences) for 20 minutes at 4°C. Between the steps, the cells were washed with PBE. The cells were further incubated with viability marker (Live Dead, Thermo Fisher Scientific) following the manufacturer's protocol and membrane marker antibodies (Supplementary Table S1) diluted in PBE for 30 minutes at 4°C. Then, the cells were washed with PBE and suspended in 4% PFA. For the detection of intracellular C1q, the anti-C1q antibody 7H8 was coupled with Cy5 using an Inova Lightning Link Rapid Cy5 Kit (342–0010) according to the manufacturer's instructions. After membrane staining, the cells were washed with Fix/Perm buffer (Thermo Fisher Scientific, 00-8333-56, 00-5223-56), permeabilized with Fix/Perm solution (Thermo Fisher Scientific, 00-5123-43, 00-5223-56) for 30 minutes at 4°C, and then stained for C1q. Finally, the cells were washed with Fix/Perm buffer. Human and mouse samples were acquired in a FACS Fortessa cytometer with FACSDiva software (BD Biosciences) and data were analyzed with FlowJo 10.0.8 software (Tree Star, Inc.).

Staining on mouse tissue. Freshly isolated mouse tumor tissues were frozen with liquid nitrogen and kept at −80°C. Tissues were cut from frozen blocks with cryostat (Leica) at a 6-μm thickness and fixed by acetone for 8 minutes. Sections were incubated with TBS, 5% BSA for 30 minutes in a humidity chamber at room temperature. Sections were incubated with primary antibody rabbit polyclonal anti-CD31 (Abcam ab124432, 10 μg/mL) or isotype for 45 minutes in TBS, 0.04% Tween20 (TTBS). Between each step, sections were washed two times for 2 minutes in TTBS. Sections were incubated with secondary antibody goat anti-rabbit IgG AF647 (Thermo Fisher Scientific, A-21245; 20 μg/mL) for 45 minutes. Sections were washed with water and incubated for 5 minutes with DAPI, and slides were mounted. Staining of other tissues (spleen, kidney, heart, and liver) was performed for controls. The slides were scanned with Zeiss Axio Scan.

Statistical analyses

The survival analyses were performed with R software version 3.4.2 and the "survival" package. The impact on survival was assessed by using Kaplan–Meier estimates and a log-rank test or by using Cox proportional hazard models, according to what is specified in the text. All survival data were censored at 2,500 days. The association between the distributions of qualitative variables was assessed by Fisher exact test. Relationships between quantitative and qualitative variables were estimated using the Mann–Whitney test. For quantitative variables, the cutoff was chosen according to the distribution curves.

Mouse tumor growth was analyzed using a two-way ANOVA test for the curve and independently each day with a nonparametric Mann–Whitney test. Data from mouse IF quantifications, flow cytometry, and qRT-PCR were analyzed using Mann–Whitney tests. These statistical analyses were performed using GraphPad Prism 6.

Results

Classical complement pathway gene expression in human cancers

By analyzing the TCGA database, we found that the genes encoding for classical complement pathway proteins were heterogeneously expressed in human cancers (Supplementary Fig. S2). ccRCC showed overexpression of all tested classical pathway genes, supporting a working hypothesis that C1q and the classical pathway play a major role in this cancer.

The density of C1q$^+$ cells is associated with poor prognosis in advanced ccRCC

C1q expression and its correlation with clinical outcome was analyzed in primary tumors from a retrospective cohort of 106 patients with stages I–IV ccRCC (Cohort 1, Table 1). We semi-quantified the density of intratumoral C1q-producing cells (Fig. 1A) as low and high, using a specific antibody (Supplementary Fig. S1A). Compared with a low density of C1q-producing cells, a high density of intratumoral C1q-producing cells had a significant negative impact on PFS ($P = 0.008$) and OS ($P = 0.0016$; Fig. 1B). When patients were stratified into early (stages I–II, Fig. 1C) and advanced (stages III–IV, Fig. 1D) cancers, the negative clinical impact of a high density of C1q$^+$ cells was evident only in patients with advanced cancers (PFS: $P = 0.004$; OS: $P = 0.002$; Fig. 1D).

This finding was validated using two independent cohorts. Cohort 2 (Table 1) included 154 patients: 68 with early (stages I–II) and 86 with advanced (stages III–IV) ccRCC. In this cohort, we had access only to PFS data and again showed the negative clinical impact of a high density of C1q$^+$ cells in advanced stage cancers (PFS: $P = 0.0109$) but not in early-stage cancers (PFS: $P = 0.527$; Fig. 1E and F). In cohort 3, composed of 43 stage IV metastatic patients with ccRCC (Table 1), we confirmed the shorter PFS ($P = 0.00276$) and OS ($P = 0.0126$; Fig. 1G) of patients having a high density of C1q$^+$ cells in their primary tumors.

TAMs are the most abundant cell type producing C1q in ccRCC

The C1q$^+$ cells were characterized by double labeling using IF (Fig. 2A–D). Cytoplasmic C1q staining was detected in infiltrating cells. We observed that some CD31$^+$ vascular endothelial cells were C1q-positive (Fig. 2A), in agreement with previous data (25), whereas the podoplanin-positive lymphatic endothelium and the SMA-positive fibroblasts were negative. Macrophages were the major cell type producing C1q in ccRCC tumors (Fig. 2B). The majority of C1q$^+$ cells expressed both CD68 and CD163 (Fig. 2B and C). Tumor cells stained negative for cytoplasmic C1q, but membranous deposits on their surface were detected in a fraction of the tumors (Fig. 2D). The density of CD163$^+$ macrophages was higher in the C1q-high tumors (Fig. 2E, $P = 3.4 \times 10^{-5}$), and quantification of the colocalization of the staining revealed that about 80% of the C1q$^+$-infiltrating cells were CD68$^+$CD163$^+$ macrophages.

Therefore, we further investigated the macrophage orientation and TME characteristics in ccRCC tumors. C1q staining showed variable intensity (by IF) among TAMs in ccRCC. A study reports that a subgroup of TAMs, specifically, CD14$^+$HLA-DR$^+$CD204$^+$CD38$^+$CD206$^-$ cells named M5, associates with exhausted T cells in ccRCC tumors (6). We reanalyzed the RNA-Seq data published by Chevrier and colleagues (6) and found significantly higher expression of *C1QA* ($P = 3.2 \times 10^{-4}$), *C1QB* ($P = 1.6 \times 10^{-4}$), and *C1QC* ($P = 1.6 \times 10^{-4}$) than in control TAMs (Fig. 2F). M5 TAMs expressed significantly higher PD-L2 (*PDCD1LG2*, $P = 1.6 \times 10^{-4}$), as well as the complement receptor for C1q *LAIR1* ($P = 6.5 \times 10^{-4}$; Fig. 2F). We further analyzed the expression of several of these genes in CD14$^+$ macrophages sorted from 7 fresh ccRCC tumors (Table 1). *C1QA* showed a significant correlation with the mRNA expression of PD-L2 (*PDCD1LG2*; $R = 0.913$, $P = 0.004$) and a trend toward a correlation with the C1q receptor *LAIR1* ($R = 0.75$, $P = 0.054$; Fig. 2G).

C1q expression is associated with immune checkpoint expression in ccRCC

Tumors from 102 patients from cohort 1 were stained for PD-1 and LAG3. A positive correlation was found between C1q$^+$ cell density and PD-1 ($P = 0.012$; Fig. 2H), as well as LAG3 ($P = 0.0008$; Fig. 2I). We also searched for a potential association between C1q expression and a T-cell signature, evaluated by *CD3*, *CD4*, and *CD8* signatures expression in public databases (TCGA), without finding a significant correlation. However, C1q gene expression correlated with that of immune exhaustion markers in ccRCC tumors in publicly available transcriptomic data from the TCGA database ($n = 537$). We found a correlation between *C1QA* gene expression and PD-L2 (*CD273* or *PDCD1LG2*, $P = 3.1 \times 10^{-56}$), as well as a correlation with PD-L1 (*CD274*, $P = 0.0003$; Fig. 2J). A correlation was also observed between *C1QA* and the immune checkpoint molecules PD-1 (*PDCD1*, $P = 1.5 \times 10^{-70}$), *LAG3* ($P = 2 \times 10^{-70}$), TIM-3 (*HAVCR2*, $P = 6.5 \times 10^{-23}$), and *CTLA4* ($P = 1.3 \times 10^{-39}$; Fig. 2K).

The classical complement pathway is activated *in situ* in ccRCC

The classical pathway can be activated by IgG-containing immune complexes. IgG staining by IF revealed IgG deposits on tumor cells, which colocalized with C1q deposits in about 30% of the cases (Fig. 3A). In the areas rich in deposits, up to 90% of the C1q deposits colocalized with IgG. The C1q deposits on tumor cells partially colocalized with the C4d staining (about half, Fig. 3B), indicating activation of the classical pathway. Membranous C1q staining outside IgG deposits was scarce, but could be related to a direct interaction of C1q with the tumor cells or with other C1q ligands. Indeed, two ccRCC cell lines, A498 and Caki-1, interacted with a C1q-coated surface at a similar level as to fibronectin (FN, positive control) and contrary to an irrelevant protein (albumin) after 10 minutes of incubation (Supplementary Fig. S3A), and the cells adhered better on C1q-coated or fibronectin-coated wells than on albumin-coated wells at 12 hours (Supplementary Fig. S3B). The higher cell density was not due to an increased proliferation rate, as measured by carboxyfluorescein succinimidyl ester method, but to better cell adherence.

Tumor cells stained positive for mRNA encoding the remaining components of the C1 complex, namely *C1R* and *C1S*, as revealed by an RNAscope assay (Fig. 3C and D). This was substantiated by expression of *C1R* and *C1S* mRNA (Supplementary Fig. S4A and S4B) and protein (Fig. 3E and F) in the human ccRCC cell lines. C4 was detected in ccRCC cell lines as measured by mRNA expression (Supplementary Fig. S4C) and at the protein level by Western blot analysis (Fig. 3G).

The native C4 protein was produced *in situ* by the tumor cells, as visualized by the colocalization of the cytoplasmic staining of cytokeratin with the staining with an anti-C4 antibody

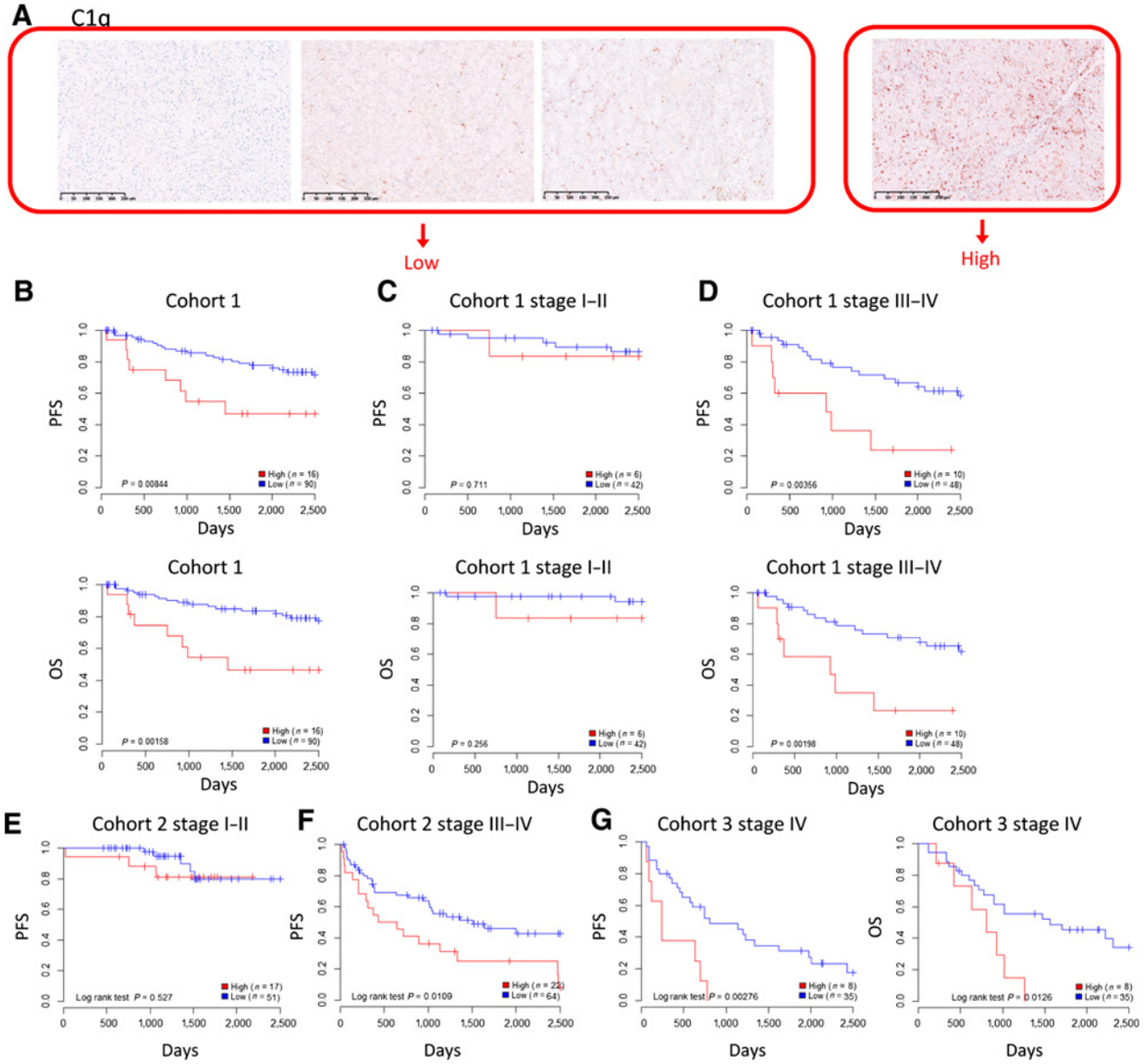

Figure 1.

The density of C1q$^+$ cells is associated with poor prognosis in advanced ccRCC. **A,** Tumor scores for C1q staining as revealed by IHC on paraffin-embedded tumor sections (200 ×). Low – less than 30% of nonneoplastic cells; High – over 30% of nonneoplastic cells. **B–D,** Kaplan–Meier curves of PFS and OS according to the C1q staining for Cohort 1 ($n = 106$). **B,** PFS and OS for the total Cohort 1. **C,** Prognostic value of C1q$^+$ cells. PFS and OS according to the presence of high or low densities of C1q$^+$ cells in Cohort 1 in localized stages I–II. **D,** PFS and OS according to the presence of high or low densities of C1q$^+$ cells in Cohort 1 in advanced stages III–IV. Prognostic value of C1q$^+$ cells on PFS of patients from Cohort 2 ($n = 154$) with localized stages I–II (**E**) and advanced stages III–IV (**F**). **G**, PFS and OS of Cohort 3 ($n = 43$) patients with high and low C1q$^+$ cell densities in metastatic stage IV. Number of patients per curve indicated on figure. Log-rank test was used and $P \leq 0.05$ was significant.

recognizing an epitope in the C4a region of the intact molecule (Fig. 3H; Supplementary Fig. S4D). Deposits of C4 activation fragments were detected on the tumor cell surface, as evidenced by using an antibody preferentially detecting C4d (Fig. 3G), colocalizing with cytokeratin (Supplementary Fig. S4E). The C4d$^+$ deposits were localized at the surface of tumor cells that could also produce C4 (Fig. 3H). Similar results were obtained for C3 (Supplementary Fig. S4F—S4H). It was produced by the ccRCC tumor cell lines at mRNA and protein level (Supplementary Fig. S4F and S4G), and C3d$^+$ deposits were detected on the surface of tumor cells of human ccRCC (Supplementary Fig. S4H).

The classical complement pathway is activated in an *in vitro* model of ccRCC

We further investigated the role of tumor cells in the formation of the C1 complex and in the activation of the classical pathway using cancer cell lines. The two ccRCC cell lines Caki-1 and A498 expressed mRNA for *C1R*, *C1S*, *C4*, and *C3* and produced their

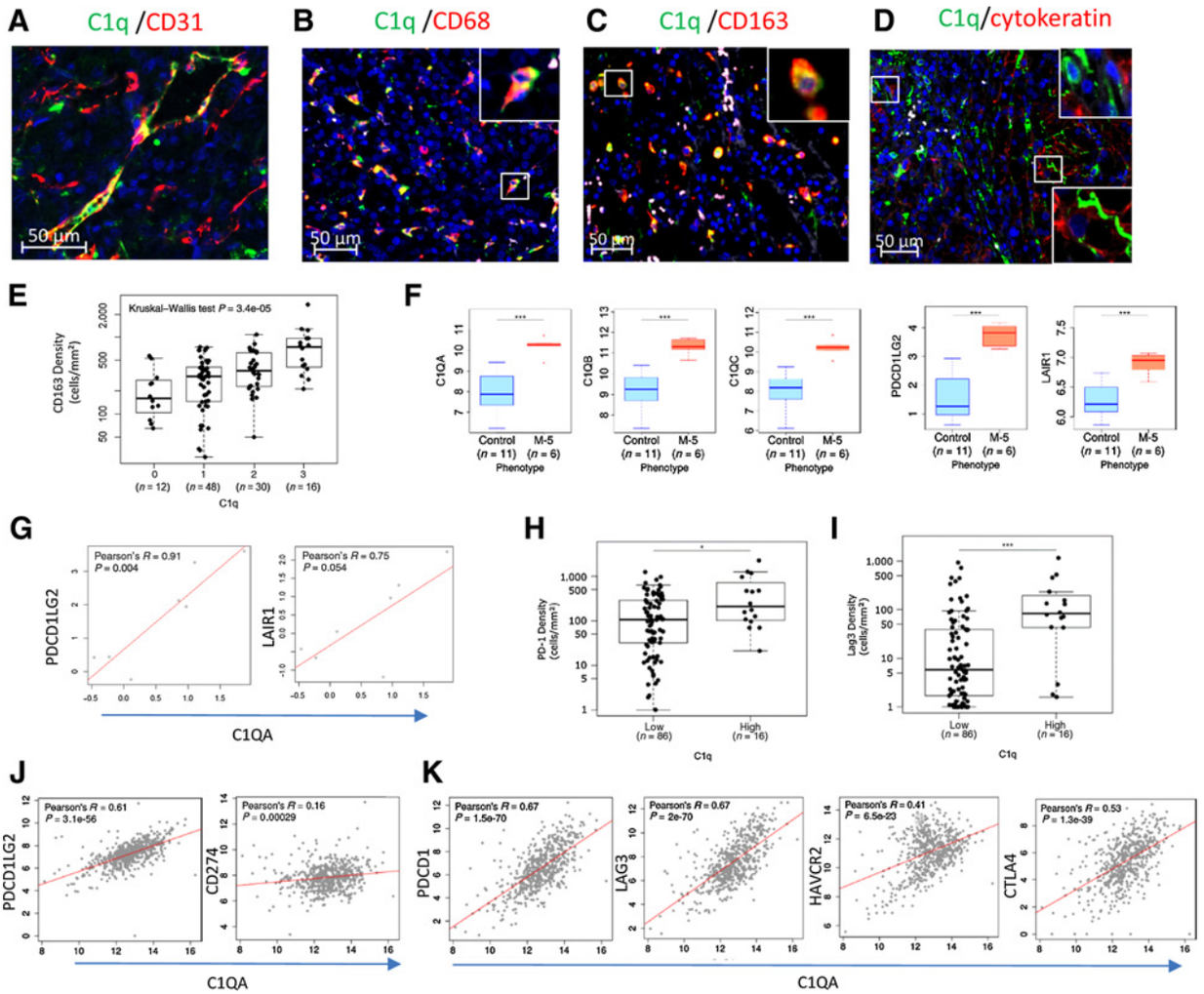

Figure 2.

C1q expression is associated with a subtype of TAMs and T-cell exhaustion. **A–D,** Identification of C1q$^+$ cells in ccRCC. ccRCC sections were double-stained for IF: C1q (green) and CD31 (endothelial cell marker, red; **A**), CD68 (macrophage marker, red; **B**), CD163 (M2 macrophage marker, red; **C**), and cytokeratin AE1/AE3 (tumoral cell marker, red; **D**). The double-positive cells appear in yellow. **D,** Double staining (top right insert) show representative intracellular C1q staining in tumor-infiltrating cells, and the lower left insert shows C1q deposits around cytokeratin$^+$ tumor cells. **E,** Densities of CD163$^+$ cells in the C1q-low (classified as 0, 1, and 2) and C1q-high (classified as 3) groups, determined by IHC in Cohort 1. Box plots represent median (wide bar) and interquartile range (IQR). Kruskal–Wallis test was used and $P \leq 0.05$ was significant. **F,** Expression of *C1QA, C1QB*, and *C1QC* mRNA in sorted M5 macrophages (CD14$^+$HLA-DR$^+$CD204$^+$CD38$^+$CD206$^-$) compared with control macrophages (CD14$^+$HLA-DR$^+$CD204$^-$CD38$^-$CD206$^-$) from ccRCC tumors according to the transcriptomic data (RNAseq) in Chevrier and colleagues (6). Gene expression of immune checkpoint PD-L2 (*PDCD1LG2*) and C1q receptor *LAIR1* in M5 versus control macrophages in the same dataset is also shown. Box plots represent median (wide bar) and IQR. Kruskal–Wallis test was used and $P \leq 0.05$ was significant. **G,** Correlation between the gene expression of *C1QA* and PD-L2 (*PDCD1LG2*) and *LAIR1* in TAMs purified from seven ccRCC fresh tumors (CD14$^+$ sorting) Pearson *R* test is used and $P \leq 0.05$ was significant. Densities of PD-1$^+$ (**H**) and Lag3$^+$ (**I**) cells in the C1q^{low} and C1q^{high} groups, determined by IHC in Cohort 1. Data were analyzed in the invasive margin and tumor core. Box plots represent median (wide bar) and IQR. Kruskal–Wallis test was used and $P \leq 0.05$ was significant. **J,** Correlation between mRNA expression of *C1QA* and *PDCD1LG2* (CD274) in the TCGA cohort ($n = 537$). Pearson *R* test was used and $P \leq 0.05$ was significant. **K,** Correlation between mRNA expression levels of *C1QA* and immune checkpoint molecules (*PDCD1, LAG3, HAVCR2, CTLA4*) in the same TCGA cohort. Pearson *R* test was used and $P \leq 0.05$ was significant.

encoded proteins, contrary to the two colon cancer cell lines (HCT116 and SW620) used as negative controls (Fig. 3E and G; Supplementary Fig. S4A–S4C, S4F, and S4G). None of these cell lines expressed detectable C1q mRNA and protein. Addition of C1r- and C1s-containing supernatants of Caki-1 and A498 to purified human C1q allowed the formation of the C1 complex (Fig. 3I), as revealed by ELISA. The first substrate of the activated C1s is C4, followed by C2. The low concentration of endogenous C4 in the supernatants precluded reliable detection of its cleavage by the C1 complex in this setting. The serine protease activity of C1s is activated when the C1 complex is assembled. To test whether the C1 complex was functionally active, exogenous purified human C1q (without C1r and C1s), C4, and C2 were added to the cancer cell line supernatants and incubated with

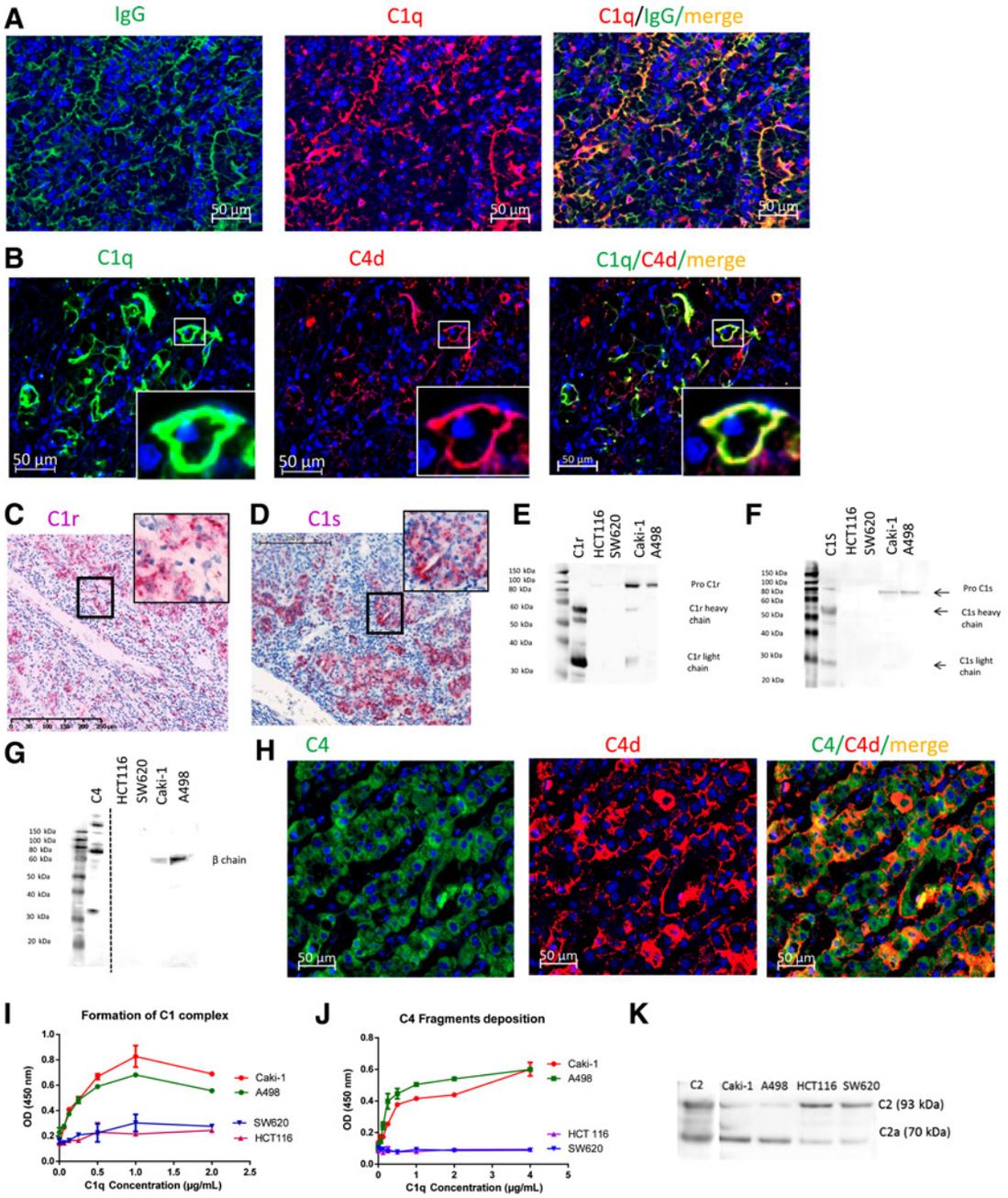

Figure 3.

The classical complement pathway is activated in ccRCC tumors. **A,** IgG deposits present in ccRCC on tumor cells. Double-staining for IF: C1q (green), IgG (red), and merged imaging (yellow). **B,** C1q and C4d deposits in ccRCC tumors of cohort 1. Double-staining with an anti-C1q (green) and an anti-C4d (red). The double-positive tumor cells appear in yellow. Detection of cells positive for *C1R* (**C**) and *C1S* (**D**) mRNA by an *in situ* hybridization RNAscope assay on paraffin-embedded ccRCC tumor sections. Detection of secreted C1r (**E**) and C1s (**F**) in the culture supernatant of ccRCC cell lines (A498 and Caki-1) compared with control cell lines (colorectal cancer cell lines HCT116 and SW620) by Western blot analysis. Human plasma-purified activated C1r and C1s were used as controls; representative image of three experiments. **G,** Detection of secreted C4 in the culture supernatant of Caki-1 and A498 compared control cell lines (colorectal cancer cell lines HCT116 and SW620) by Western blot analysis. **H,** Tumor cell C4 and C4d deposits in ccRCC tumors of cohort 1. Double-staining with an anti-C4a (green) and an antibody preferentially recognizing C4d and activated fragments of C4 in red. The double-positive cells appear in yellow. **I,** Formation of the C1 complex in supernatants of ccRCC (A498 and Caki-1) and control (SW620 and HCT116) cell lines after the addition of purified human C1q, revealed by ELISA (mean±SD; experiments performed in triplicate; representative results of three independent experiments). **J** and **K,** Evaluation of the activity of the C1 complex formed (as in **I**); (mean ± SD; samples tested in triplicate; representative results of two independent experiments). **J,** The preformed C1 complex ($C1q^+$ cell supernatant) was allowed to interact with the IgG-coated surface. Purified C4 and C2 were added to the wells, and C4 activation fragment deposition was detected by ELISA. **K,** C2 cleavage by the C1q complex. Supernatants from the experiment in **J** were recovered and resolved on gels to detect the C2 fragment generation.

surface-immobilized IgG, as a model of immune complexes. C4 activation fragment deposition (Fig. 3J) and cleavage of C2 (Fig. 3K) were detected in the presence of the ccRCC cell line supernatants, contrary to the control supernatants, demonstrating that the formed C1 complex was functionally active. The ccRCC cell lines had high expression of membrane complement regulators, such as CD46, CD55, and CD59 (Supplementary Fig. S5A–S5C), as well as soluble ones, like Factor H and Factor I (Supplementary Fig. S5D and S5E), which can protect them from the formation of cytotoxic membrane attack complex C5b-9.

The density of $C4^+$ and $C3^+$ cells and $C4d^+$ deposits correlates with poor prognosis

We semiquantified the density of C4- (Fig. 4A) and C3-producing (Supplementary Fig. S6A) tumor cells in cohort 1 (106 patients, Table 1). Patients with tumors having a high density of C4-producing tumor cells had significantly decreased PFS (Fig. 4B, left, $P = 0.02$) and OS (Fig. 4B, right; $P = 0.03$). Similarly, the density of C3-producing tumor cells (Supplementary Fig. S6A and S6B) showed a significant association with shorter PFS (Supplementary Fig. S6B, left; $P = 0.035$) and a trend toward association with shorter OS (Supplementary Fig. S6B, right; $P = 0.07$).

Comparing low and high staining scores for C4 activation fragment deposits (Fig. 4C) revealed a significant association with poor prognosis for the high group for both PFS (Fig. 4D, left; $P = 0.013$) and OS (Fig. 4D, right; $P = 0.007$). Combining the densities of C4-producing cells and C4 deposits yielded a deleterious prognosis for both PFS and OS ($P = 0.018$ and $P = 0.0036$, respectively) in the group of patients with high C4-producing cells and high deposits (Fig. 4E). The C3 activation fragment deposits did not correlate with survival (Supplementary Fig. S6C and S6D).

Correlation between local production and complement deposits in patients with ccRCC

C1q deposits correlated with the deposits of C4 activation fragments in the tumors from Cohort 1 (Supplementary Fig. S7A, $P = 0.031$). Cytoplasmic staining and deposits of C3 (Supplementary Fig. S7B and S7C) correlated with the C1q and C4 activation fragment deposition ($P = 0.002$ and $P = 0.001$, respectively). The local production of C4 and C3, revealed by the cytoplasmic staining in the tumor cells, was correlated with the local deposits (Supplementary Fig. S7D and S7E; $P = 0.033$ for C4 and $P = 0.018$ for C3).

Complement is an independent prognostic factor in ccRCC

Finally, univariate Cox proportional hazards models were fitted for clinicopathologic parameters (sex, age, stage, Fuhrman grade, and presence of a sarcomatoid component), as well as complement-related variables for both PFS and OS (Table 2). All variables significantly associated with prognosis were then integrated into multivariate models integrating either all complement-associated variables or C1q. The prognostic impact of C1q on PFS and OS was found to be independent from clinical parameters (Fuhrman grade, TNM stage, and sarcomatoid component; $P = 0.014$ and $P = 0.007$, respectively). In contrast, C1q was not an independent marker when the remaining complement-related parameters were incorporated, probably because of the correlation of complement-associated variables.

Ablation of C1q, C4, and C3 in mice is associated with decreased tumor growth

To evaluate the impact of C1q and the classical complement pathway activation *in vivo*, we analyzed tumor models in $C1q^{-/-}$ mice on the C57BL/6 background. We searched for syngeneic tumor models, in which the tumor cells produce C1r, C1s, C3, and C4 and in which C1q could be present in the TME. In the absence of RCC models growing in C57BL/6 mice, we screened five tumor cell lines and found that they expressed detectable *C1r* and *C1s* at the mRNA level (Fig. 5A) but not *C1q* or *Mbl2* (MBL), similarly to the human ccRCC cell lines. These cell lines also had a heterogeneous expression of *C4*, *C3*, and *C2*. We selected the TC-1 cell line because it expressed all the genes of interest and represented a model where complement activation contributes to tumor growth (11).

Intracellular staining for C1q from harvested tumors by flow cytometry showed that a minority of $CD45^-$ cells were $C1q^+$ (presumably endothelial cells; Fig. 5B, left). Positivity was detected in dendritic cells (DC; $CD45^+CD3^-CD11b^+CD11c^+$), but they represented only approximately 5% of the $CD45^+$ cells (Fig. 5B, middle). The major C1q-expressing population in the TC-1 tumors were the macrophages ($CD45^+CD3^-CD11b^+CD11c^-Ly6C^{low}Ly6G^-$ Fig. 5B, right) representing approximately 60% of the $CD45^+$ cells at an early timepoint (day 10).

To establish whether activation of the early steps of the complement cascade could be involved in tumor progression, we grafted TC-1 cells into $C3^{-/-}$, $C4^{-/-}$, and $C1q^{-/-}$ mice. The $C3^{-/-}$ mice were nearly completely protected from tumor growth in these experimental settings, (Fig. 5C) and a significant reduction of the tumor size in $C4^{-/-}$ mice was seen (Fig. 5D) for the late time points, in agreement with previous observations (11). After day 15 in $C1q^{-/-}$ mice, TC-1 tumors were significantly smaller than those grafted into WT mice (Fig. 5E), demonstrating the implication of the early steps of complement activation in tumor progression.

Impact of C1q on neoangiogenesis

C1q is reported to impact neoangiogenesis in mouse tumor models (26). Indeed, we detected a difference in the morphology of the vasculature between tumors growing in $C1q^{-/-}$ mice and those growing in WT mice in the TC-1 model (Supplementary Fig. S8A). Tumors growing in $C1q^{-/-}$ mice exhibited shorter vessels with disrupted organization (data shown for day 17). In contrast, the staining of tumors from $C4^{-/-}$ mice did not show a difference compared with tumors in WT mice (Supplementary Fig. S8B). In human ccRCC, no correlation was observed between *C1QA* gene expression and the endothelial cell signature, defined by the MCP-counter approach (18), in the TCGA cohort and in our cohort 3 (Supplementary Fig. S8C). The presence of C1q-positive staining in vessels did not affect survival. Nevertheless, among the neoangiogenesis-related genes tested, *VEGFC* showed a positive correlation with *C1QA* gene in both cohorts (TCGA: $r = 0.412$, $P = 7.10^{-24}$, Cohort 3: $r = 0.141$, $P = 0.00075$; Supplementary Fig. S8D). The *Vegfc* gene expression was downregulated in the tumors of $C1q^{-/-}$ mice compared with tumors from WT mice (Supplementary Fig. S8E).

Discussion

Here, we described the protumoral properties of a population of TAMs expressing C1q in ccRCC. TAM-derived C1q is hijacked by the cancer cells, which produced C1r, C1s, C4, and C3 to

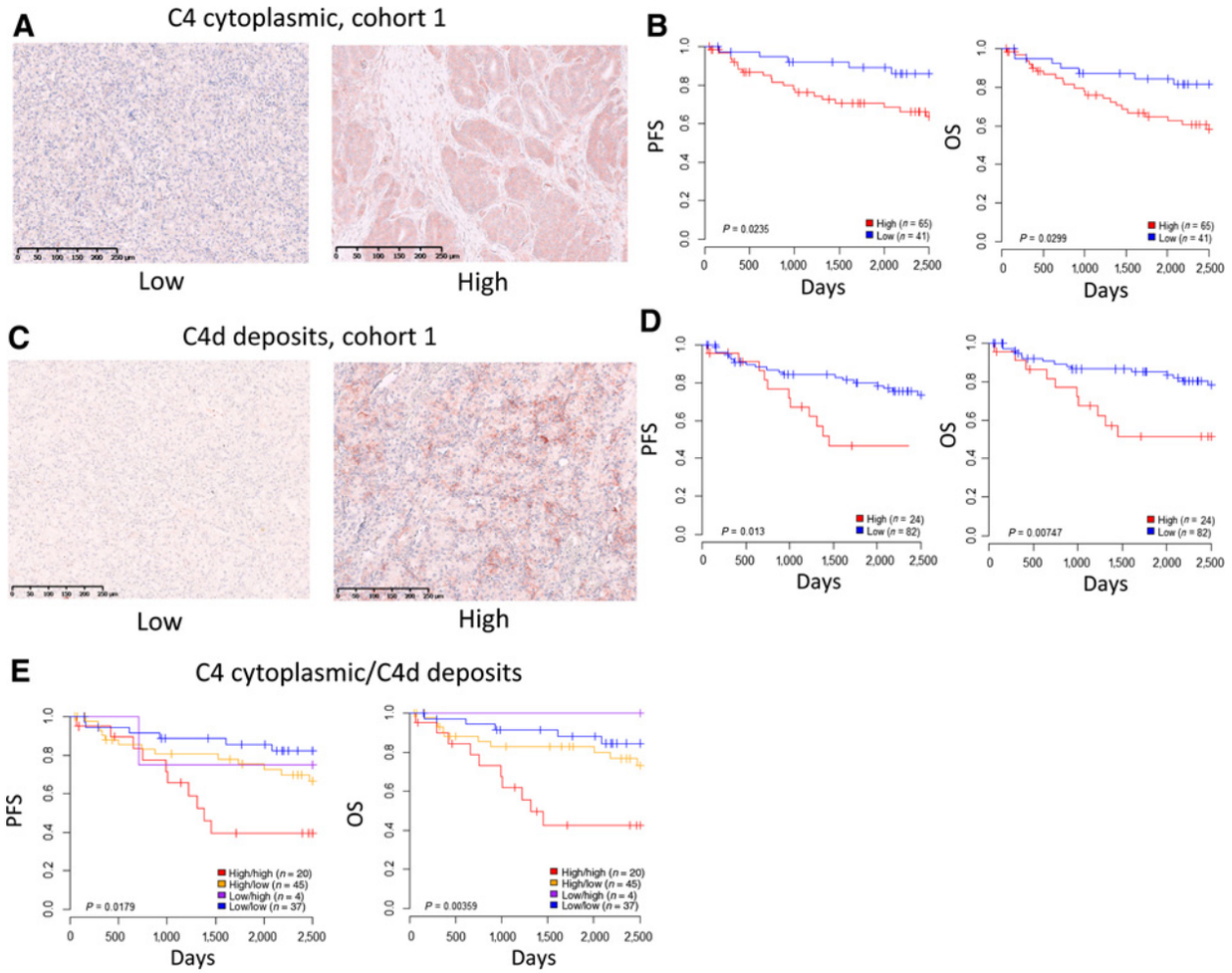

Figure 4.

The density of $C4^+$ cells and C4 activation fragment deposits are associated with poor prognosis in ccRCC. **A,** Tumor scores for C4 cytoplasmic staining of tumor cells (low: below 30% of the tumor cells, high: over 30% positive tumor cells) revealed by IHC on paraffin-embedded tumor sections for Cohort 1. **B,** Kaplan–Meier curves of PFS and OS according to C4 cytoplasmic staining on tumor cells for cohort 1. Log-rank test was used and $P \leq 0.05$ was significant. **C,** Tumor classification for C4d deposits on tumor cells (0: <1%, 1: 1–30%, 2: >30% positive cells) as revealed by IHC on paraffin-embedded tumor sections. Tumors were classified as low or high for C4d deposits. **D,** Kaplan–Meier curves of PFS and OS according to C4d deposits on tumor cells for Cohort 1. Log-rank test was used and $P \leq 0.05$ was significant. **E,** Kaplan–Meier curves according to combined intensities of cytoplasmic C4 staining and C4d deposits for Cohort 1. Log-rank test was used and $P \leq 0.05$ was significant. Number of patients per curve indicated on figure.

initiate the classical pathway of the complement cascade on intratumoral IgG immune complexes. Inflammation and T-cell exhaustion, promoted by C1q-expressing TAMs and complement activation products, fueled tumor progression. We identified C1q-expressing TAMs and $C4d^+$ deposits at high densities on tumor cells as markers for deleterious prognosis in ccRCC.

C1q is a multifunctional molecule, activating the classical complement pathway and acting outside the cascade as a modulator of the phenotype of immune cells, as a mediator of immune tolerance in apoptotic cell clearance, as an angiogenic factor, and/or as a modulator of cell proliferation (27, 28). C1q can be produced by the M2 macrophages, and it favors M2 polarization *in vitro*, independently of its actions within the cascade (29, 30). C1q also inhibits $CD8^+$ T-cell activation, proliferation, and cytotoxic functions under suboptimal stimulation *in vitro* (31), a situation that may occur in the TME.

We found that in ccRCC, C1q is produced mainly by the TAMs and that the high density of C1q-producing cells is a robust marker for unfavorable prognosis in advanced stages of ccRCC (III and IV) in three independent cohorts. To find out the mechanism behind this association, we studied the main functions of C1q, namely its capacity to activate complement, to promote neoangiogenesis, and to modulate the phenotype of T cells.

A major factor affecting tumor growth is the phenotype of TAMs and tumor-infiltrating T cells. M2 macrophages are considered as having a tumor-promoting phenotype in renal cancer (3, 32). We found that C1q is produced mainly by a subset of TAMs in ccRCC, which belong to the large class of the M2 ($CD163^+$) macrophages. Reanalyzing the transcriptomic profile of reported M5 macrophages (6), we noticed high expression of C1q-related genes, suggesting that this subtype could be the main source of C1q in ccRCC. These TAMs also had higher expression C1q receptors and

Table 2. Univariate and multivariate analysis of PFS and OS in patients with ccRCC, Cohort 1

	Univariate		Multivariate		Multivariate C1q vs. clinical data	
Progression-free survival	**HR (95% CI)**	***P***	**HR (95% CI)**	***P***	**HR (95% CI)**	***P***
Sex, Male vs. Female	1.000 (0.45–2.25)	0.994				
Age	1.030 (0.99–1.06)	0.115				
Stage.UICC.1997 III/IV vs. I/II	4.31 (0.23–1.76)	**0.00141**	2.902 (1.14–7.42)	0.261	2.838 (1.11–7.25)	**0.0292**
Fuhrman Grade 3/4 vs. 1/2	7.11 (1.70-29.89)	**0.00742**	4.094 (0.92–18.28)	0.649	4.860 (1.12–21.07)	**0.0346**
Sarcomatoid	3.95 (1.73-9.00)	**0.00109**	1.791 (0.74–4.33)	0.195	2.075 (0.88–4.88)	**0.0945**
C1q High vs. Low	2.855 (1.26–6.46)	**0.0118**	2.122 (0.84–5.34)	0.11	2.861 (1.23–6.63)	**0.0142**
C4 Production High vs. Low	2.477 (1.06-5.78)	**0.0359**	1.230 (0.50–3.02)	0.652		
C4d Deposit High vs. Low	2.5 (1.18–5.28)	**0.0164**	1.480 (0.64–3.40)	0.356		
C3 Production High vs. Low	2.243 (1.03-4.90)	**0.0428**	1.356 (0.59–3.13)	0.476		
C3d Deposit High vs. Low	0.867 (0.35–2.13)	0.758				

	Univariate		Multivariate		Multivariate C1q vs. clinical data	
OS	**HR (95% CI)**	***P***	**HR (95% CI)**	***P***	**HR (95% CI)**	***P***
Sex, Male vs. Female	1.156 (0.46–2.89)	0.757				
Age	1.023 (0.99–1.06)	0.193				
Stage.UICC.1997 III/IV vs. I/II	7.908 (2.36–26.46)	**0.000791**	5.024 (1.45–17.45)	0.0111	5.034 (1.45–17.48)	**0.0109**
Fuhrman grade 3/4 vs. 1/2	12.12 (1.64–89.69)	**0.0146**	6.805 (0.87–53.30)	0.068	7.345 (0.96–56.12)	**0.0546**
Sarcomatoid	4.042 (1.66-9.84)	**0.00208**	1.579 (0.32–4.03)	0.339	1.870 (0.75–4.65)	0.1779
C1q High vs. Low	3.605 (1.54-8.43)	**0.0031**	2.791 (1.04-7.49)	0.041	3.333 (1.39–8.03)	**0.0072**
C4 Production High vs. Low	2.947 (1.10–7.86)	**0.0309**	1.373 (0.48–3.92)	0.554		
C4d Deposit High vs. Low	2.859 (1.28–6.39)	**0.0106**	1.544 (0.63–3.80)	0.345		
C3 Production High vs. Low	1.706 (0.75–3.86)	0.2	0.876 (0.35–2.16)	0.774		
C3d Deposit High vs. Low	0.879 (0.33–2.34)	0.796				

NOTE: The *P*-values reaching statistical significance are in bold.

C3aR, making them responsive to C1q and C3a. TAMs also overexpressed PD-L2. It is tempting to speculate that M5 macrophages exert their immunosuppressive activity via the action of C1q. Indeed, it was shown that C1q, in the context of phagocytosis of dying cells, induces a tolerogenic/immunosuppressed phenotype in macrophages *in vitro*, which is associated with the upregulation of PD-L1 and PD-L2, as well as reduced proliferation of T cells (33). C1q also exert direct effects on T cells by inhibiting their proliferation (34) and by modulation of the mitochondrial metabolism of $CD8^+$ T cells, restraining their activation (31). Herein, ccRCC tumors with the highest C1q expression were enriched in $PD\text{-}1^+$ and $LAG3^+$ cells, suggesting immune suppression/T-cell exhaustion. This was confirmed at the gene expression level in ccRCC tumors from the TCGA database. Altogether, these results point toward an (autocrine) mechanism by which a subtype of TAMs produce C1q, which contributes to PD-L1 and PD-L2 expression and subsequent T-cell exhaustion. These data demonstrated the importance of C1q for the phenotype of TAMs and their interaction with the T-cell subsets. The role of complement anaphylatoxins in this process requires further studies.

The contribution of complement to cancer progression is a complex phenomenon. Data support the protumoral effects of C3a/C3aR and C5a/C5aR axes in experimental models and patients (13), but little is known about the complement activation pathways and their triggers (35). The most detailed characterization of the protumoral effect of C5a/C5aR axis was done using the TC-1 mouse tumor model, but the initiation mechanisms were not described (11). We found that the TC-1 tumor cells express a similar set of classical pathway genes as the ccRCC tumor cells and that the TAMs from this model produced C1q. The TC-1 tumors had a slower progression in $C1q^{-/-}$, $C4^{-/-}$, and $C3^{-/-}$ mice, demonstrating the protumoral properties of C1q and the classical pathway *in vivo*. The protective effect of the C3 deficiency was more pronounced compared with $C1q^{-/-}$ and $C4^{-/-}$. Bonavita and colleagues showed that $C3^{-/-}$ mice develop smaller tumors in a carcinogen-induced sarcoma model, providing a genetic evidence for the protective role of the C3 deficiency in carcinogenesis (36). The intratumoral activation of the alternative pathway could play a role, as well as the intracellular, noncanonic functions of C3. Noncanonical intracellular tumor cell–derived C3 activation also suppresses antitumor immunity (37).

In mice, C1q has a critical role in promoting neoangiogenesis (25, 26, 38, 39). It is important to note that ccRCC is a very highly vascularized tumor, due to the dominant effect of the VHL mutation, (40) and therefore, the role of C1q on the angiogenesis may not be visible in this tumor type. Renal endothelium shows unique features, lacking in other vascular beds (41). However, despite the lack of correlation between the C1q genes and the endothelial cell signature, a link with the expression of *VEGFC* both in patients and in the mouse model was seen. The intratumoral vascular network was disorganized in the tumors from $C1q^{-/-}$ mice. This pattern was not observed in $C4^{-/-}$, suggesting a noncanonical function of C1q outside of the complement cascade, likely related to *VEGFC*.

ccRCC is particular in its capacity to express components of the classical complement pathway. We found a correlation between the local production and deposition of complement in this cancer. The classical complement pathway requires a trigger. Dying cells or pentraxins could serve as C1q-binding targets, but the most common ones are IgG- and IgM-containing immune complexes (41–44). We detected the presence of IgG deposits on tumor cells in ccRCC. IgG colocalized with C1q deposits and C1q deposits with C4d, showing that all elements needed for classical pathway activation coincided spatially and temporarily in ccRCC. C1q bound directly to the tumor cells of ccRCC *in situ* and *in vitro*, in agreement with observations for other cancer cell lines (26, 39, 45). This suggests a possible activation of complement, independently of immune complexes. Therefore, classical pathway initiators are present in ccRCC. Tumor cells and cell lines produced C1r and C1s that could assemble with C1q, enabling the formation of a functional C1 complex and complement activation in ccRCC tumors. Tumor cells were the local source of C4 and C3.

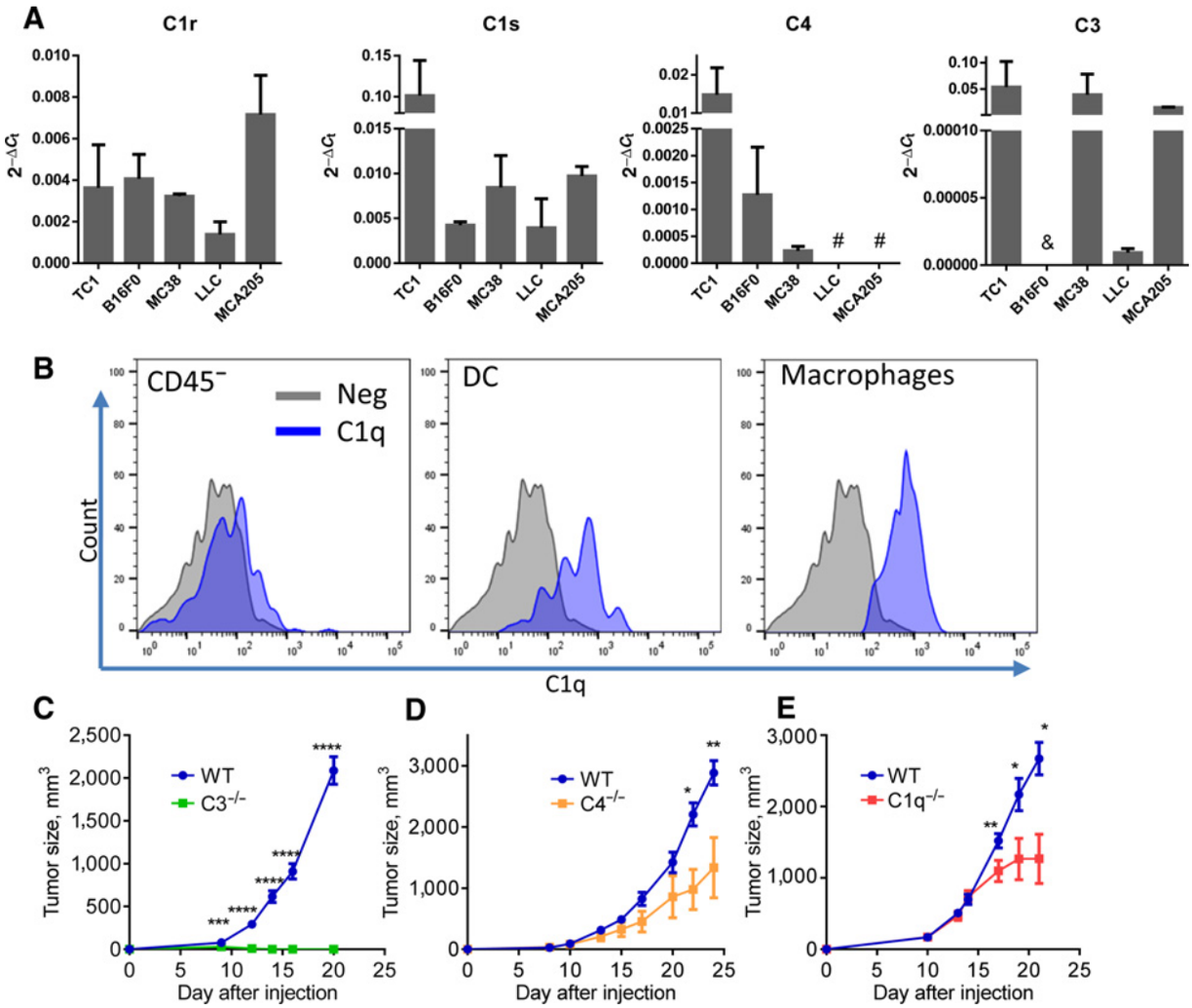

Figure 5.

C1q and the classical pathway are implicated in tumor progression in a mouse model of tumor progression. **A,** Expression of complement genes by murine cancer cell lines TC-1, B16F0, MC38, LLC, and MCA205 (mean ± SD, $n = 4$ independent experiments). Data for C1r, C1s, C4, and C3 shown. C1qA, C1qB, C1qC, and Mbl2 genes showed no expression. **B,** Flow cytometry analyses of the C1q-producing cells in the tumors after injection of the selected TC-1 cells. Intracellular staining for C1q in $CD45^-$ cells (left), DCs (middle), and TAMs (right; day 10). **C–E,** Tumor growth after subcutaneous injection of TC-1 tumor cells into WT and complement-deficient mice. At each timepoint the groups were compared (Mann–Whitney, *, $P \leq 0.05$; **, $P \leq 0.01$, ***, $P \leq 0.001$, ****, $P \leq 0.0001$). **C,** WT versus $C3^{-/-}$ mice (mean ± SEM; $n = 10$ WT and $n = 10$ $C3^{-/-}$ mice/group; representative experiment out of two performed). **D,** WT versus $C4^{-/-}$ mice (mean ± SEM; $n = 10$ WT and $n = 9$ $C4^{-/-}$ mice/group; one out of two experiments performed). **E,** WT versus $C1q^{-/-}$ mice (mean ± SEM; $n = 20$ WT and $n = 18$ $C1q^{-/-}$ mice/group; representative experiment, six other experiments performed with 5–10 mice/group).

C3 and C4 were cleaved, and their activation fragments were deposited on tumor cell membranes, reflecting complement activation. Indeed, our results suggest that the deleterious effect of C4 on clinical outcome was due to its activation and deposition, rather than only its production, similar to observations in lung cancer (46, 47). The local production of C3 was also associated with poor outcome, but the C3 activation fragment deposits did not show prognostic value. We hypothesize that this finding could be due to the large variety of C3 activation fragments that may be present on the cell surface (C3b, iC3b, and C3d), each having opposing functions both on the complement cascade and on immune cells (10). Taken together, our results in ccRCC and in the mouse model demonstrated that classical complement pathway activation occurs in cancer and has a protumoral effect. Our data fit with the findings that positive C5a/C5aR staining is associated with a poor prognosis in ccRCC (48, 49), and genetic partial C4 deficiency is related to prolonged survival (50), hinting that complement activation could promote tumor growth. Our data indicate that the local production of complement components is mandatory for the efficient, cancer-promoting activation of the complement cascade. However, this complement activation does not end up in cell killing, most likely due to the strong expression of complement regulators.

In conclusion, classical complement pathway activation occurs in human ccRCC through the orchestrated production of C1q by TAMs and other complement components by cancer

cells. This unique cooperative activation process fuels inflammation and has a deleterious impact on patients' prognosis. These results open the gateway for designing novel therapeutic strategies in ccRCC.

Disclosure of Potential Conflicts of Interest

L.T. Roumenina reports receiving a commercial research grant from the Pierre Fabre Research Institute. E. Chetaille is the head of the Oncology Innovation Unit at Pierre Fabre. W.H. Fridman reports receiving a commercial research grant from Pierre Fabre Medicaments and is a consultant/advisory board member for Pierre Fabre Medicaments. No potential conflicts of interest were disclosed by other authors.

Authors' Contributions

Conception and design: L.T. Roumenina, M.V. Daugan, Y.A. Vano, E. Becht, N.A. Giraldo, C.-M. Sun, P. Ferré, N. Corvaia, C. Sautes-Fridman, W.H. Fridman
Development of methodology: L.T. Roumenina, M.V. Daugan, R. Noé, B. Le Clec'h, N.A. Giraldo, N.S. Merle, L. Lacroix, C. Thuilliez, A. de Reynies
Acquisition of data (provided animals, acquired and managed patients, provided facilities, etc.): M.V. Daugan, R. Noé, Y.A. Vano, R. Sanchez-Salas, B. Le Clec'h, N.A. Giraldo, C.-M. Sun, V. Verkarre, P. Validire, J. Selves, L. Lacroix, I.B. Sakhi, M. Botto, A. Mejean, X. Cathelineau
Analysis and interpretation of data (e.g., statistical analysis, biostatistics, computational analysis): L.T. Roumenina, M.V. Daugan, R. Noé, F. Petitprez, E. Becht, J. Meilleroux, B. Le Clec'h, N.A. Giraldo, N.S. Merle, O. Delfour, I. Vandenberghe, S. Keddani, I.B. Sakhi, N. Corvaia, E.Chetaille, C. Sautes-Fridman, W.H. Fridman
Writing, review, and/or revision of the manuscript: L.T. Roumenina, M.V. Daugan, R. Noé, F. Petitprez, Y.A. Vano, E. Becht, N.A. Giraldo, I.B. Sakhi, E. Barret, A. Passioukov, E.Chetaille, M. Botto, A. de Reynies, S.M. Oudard, C. Sautes-Fridman, W.H. Fridman
Administrative, technical, or material support (i.e., reporting or organizing data, constructing databases): R. Sanchez-Salas, L. Lacroix, S. Keddani
Study supervision: L.T. Roumenina, N. Corvaia, E. Chetaille, A. Mejean, C. Sautes-Fridman, W.H. Fridman

Acknowledgments

We thank Veronique Fremeaux-Bacchi (CRC) for the stimulating discussions as well as Alexia Tavares, Jennifer Tardiveau, Carine Torset, Sarah Bourass, Ivo Natario, Benedicte Buttard, Margot Revel, and Natalie Jupiter at Cordeliers Research Center (CRC) for their technical assistance. The slides stained for IF were scanned and analyzed at the Centre d'Histologie, d'Imagerie et de Cytométrie (CHIC), Centre de Recherche des Cordeliers UMRS1138 (Paris, France). CHIC is a member of the Sorbonne University Flow Cytometry Network (RECYF). We are grateful for the excellent technical assistance of the CHIC, CEF, and CGB crew of Centre de Recherche des Cordeliers for their support with the imaging and animal experimentation. We thank Isabelle Sauret and Simon Lefranc from Centre de Ressources Biologiques and the Pathology Department at the IMM for their help in the sample storage and collection. This work was supported by a grant from Pierre Fabre Research Institute (to W.H. Fridman and L.T. Roumenina), grants from Association pour la Recherche sur le Cancer (ARC) and Cancer Research for Personalized Medicine (CARPEM; to L.T. Roumenina); La Ligue contre le cancer (RS19/75-111 to L.T. Roumenina); Institut du Cancer (INCa) HTE Plan Cancer (C1608DS to C. Sautes-Fridman), PRTK G26 NIVOREN and BioniKK (to C. Sautes-Fridman) programs. This work was also supported by INSERM, University Paris Descartes, Sorbonne University, CARPEM T8, and the Labex Immuno-Oncology Excellence Program. M.V. Daugan received a PhD fellowship from ARC. F. Petitprez and Y.A.Vano were supported by CARPEM doctorate fellowships.

The costs of publication of this article were defrayed in part by the payment of page charges. This article must therefore be hereby marked *advertisement* in accordance with 18 U.S.C. Section 1734 solely to indicate this fact.

Received December 14, 2018; revised March 1, 2019; accepted May 30, 2019; published first June 4, 2019.

References

1. Frew IJ, Moch H. A clearer view of the molecular complexity of clear cell renal cell carcinoma. Annu Rev Pathol 2015;10:263–89.
2. Giraldo NA, Becht E, Pages F, Skliris G, Verkarre V, Vano Y, et al. Orchestration and prognostic significance of immune checkpoints in the microenvironment of primary and metastatic renal cell cancer. Clin Cancer Res 2015;21:3031–40.
3. Komohara Y, Hasita H, Ohnishi K, Fujiwara Y, Suzu S, Eto M, et al. Macrophage infiltration and its prognostic relevance in clear cell renal cell carcinoma. Cancer Sci 2011;102:1424–31.
4. Mantovani A, Sozzani S, Locati M, Allavena P, Sica A. Macrophage polarization: tumor-associated macrophages as a paradigm for polarized M2 mononuclear phagocytes. Trends Immunol 2002;23:549–55.
5. Ginhoux F, Guilliams M. Tissue-resident macrophage ontogeny and homeostasis. Immunity 2016;44:439–49.
6. Chevrier S, Levine JH, Zanotelli VRT, Silina K, Schulz D, Bacac M, et al. An immune atlas of clear cell renal cell carcinoma. Cell 2017;169:736–49.
7. Fridman WH, Pages F, Sautes-Fridman C, Galon J. The immune contexture in human tumours: impact on clinical outcome. Nat Rev Cancer 2012;12:298–306.
8. Miao D, Margolis CA, Gao W, Voss MH, Li W, Martini DJ, et al. Genomic correlates of response to immune checkpoint therapies in clear cell renal cell carcinoma. Science 2018;359:801–6.
9. Fridman WH, Zitvogel L, Sautes-Fridman C, Kroemer G. The immune contexture in cancer prognosis and treatment. Nat Rev Clin Oncol 2017;14:717–34.
10. Merle NS, Noe R, Halbwachs-Mecarelli L, Fremeaux-Bacchi V, Roumenina LT. Complement system part II: role in immunity. Front Immunol 2015;6:257.
11. Markiewski MM, DeAngelis RA, Benencia F, Ricklin-Lichtsteiner SK, Koutoulaki A, Gerard C, et al. Modulation of the antitumor immune response by complement. Nat Immunol 2008;9:1225–35.
12. Afshar-Kharghan V. The role of the complement system in cancer. J Clin Invest 2017;127:780–9.
13. Reis ES, Mastellos DC, Ricklin D, Mantovani A, Lambris JD. Complement in cancer: untangling an intricate relationship. Nat Rev Immunol 2018;18:5–18.
14. Roumenina LT, Rayes J, Frimat M, Fremeaux-Bacchi V. Endothelial cells: source, barrier, and target of defensive mediators. Immunol Rev 2016;274:307–29.
15. Morgan BP, Gasque P. Extrahepatic complement biosynthesis: where, when and why? Clin Exp Immunol 1997;107:1–7.
16. Zhou W, Marsh JE, Sacks SH. Intrarenal synthesis of complement. Kidney Int 2001;59:1227–35.
17. Uhlen M, Zhang C, Lee S, Sjostedt E, Fagerberg L, Bidkhori G, et al. A pathology atlas of the human cancer transcriptome. Science 2017;357:pii: eaan2507.
18. Becht E, Giraldo NA, Lacroix L, Buttard B, Elarouci N, Petitprez F, et al. Estimating the population abundance of tissue-infiltrating immune and stromal cell populations using gene expression. Genome Biol 2016;17:218.
19. Beuselinck B, Job S, Becht E, Karadimou A, Verkarre V, Couchy G, et al. Molecular subtypes of clear cell renal cell carcinoma are associated with sunitinib response in the metastatic setting. Clin Cancer Res 2015;21:1329–39.
20. Roumenina LT, Sene D, Radanova M, Blouin J, Halbwachs-Mecarelli L, Dragon-Durey MA, et al. Functional complement C1q abnormality leads to impaired immune complexes and apoptotic cell clearance. J Immunol 2011;187:4369–73.
21. Roumenina LT, Radanova M, Atanasov BP, Popov KT, Kaveri SV, Lacroix-Desmazes S, et al. Heme interacts with c1q and inhibits the classical complement pathway. J Biol Chem 2011;286:16459–69.
22. Botto M, Dell'Agnola C, Bygrave AE, Thompson EM, Cook HT, Petry F, et al. Homozygous C1q deficiency causes glomerulonephritis associated with multiple apoptotic bodies. Nat Genet 1998;19:56–9.
23. Petry F, McClive PJ, Botto M, Morley BJ, Morahan G, Loos M. The mouse C1q genes are clustered on chromosome 4 and show conservation of gene organization. Immunogenetics 1996;43:370–6.

24. Lin KY, Guarnieri FG, Staveley-O'Carroll KF, Levitsky HI, August JT, Pardoll DM, et al. Treatment of established tumors with a novel vaccine that enhances major histocompatibility class II presentation of tumor antigen. Cancer Res 1996;56:21–6.
25. Bulla R, Agostinis C, Bossi F, Rizzi L, Debeus A, Tripodo C, et al. Decidual endothelial cells express surface-bound C1q as a molecular bridge between endovascular trophoblast and decidual endothelium. Mol Immunol 2008; 45:2629–40.
26. Bulla R, Tripodo C, Rami D, Ling GS, Agostinis C, Guarnotta C, et al. C1q acts in the tumour microenvironment as a cancer-promoting factor independently of complement activation. Nat Commun 2016;7:10346.
27. Ugurlar D, Howes SC, de Kreuk BJ, Koning RI, de Jong RN, Beurskens FJ, et al. Structures of C1-IgG1 provide insights into how danger pattern recognition activates complement. Science 2018;359:794–7.
28. Thielens NM, Tedesco F, Bohlson SS, Gaboriaud C, Tenner AJ. C1q: a fresh look upon an old molecule. Mol Immunol 2017;89:73–83.
29. Armbrust T, Nordmann B, Kreissig M, Ramadori G. C1Q synthesis by tissue mononuclear phagocytes from normal and from damaged rat liver: up-regulation by dexamethasone, down-regulation by interferon gamma, and lipopolysaccharide. Hepatology 1997;26:98–106.
30. Benoit ME, Clarke EV, Morgado P, Fraser DA, Tenner AJ. Complement protein C1q directs macrophage polarization and limits inflammasome activity during the uptake of apoptotic cells. J Immunol 2012;188: 5682–93.
31. Ling GS, Crawford G, Buang N, Bartok I, Tian K, Thielens NM, et al. C1q restrains autoimmunity and viral infection by regulating CD8(+) T cell metabolism. Science 2018;360:558–63.
32. Dannenmann SR, Thielicke J, Stockli M, Matter C, von Boehmer L, Cecconi V, et al. Tumor-associated macrophages subvert T-cell function and correlate with reduced survival in clear cell renal cell carcinoma. Oncoimmunology 2013;2:e23562.
33. Clarke EV, Weist BM, Walsh CM, Tenner AJ. Complement protein C1q bound to apoptotic cells suppresses human macrophage and dendritic cell-mediated Th17 and Th1 T cell subset proliferation. J Leukoc Biol 2015;97: 147–60.
34. Ghebrehiwet B, Lu PD, Zhang W, Keilbaugh SA, Leigh LE, Eggleton P, et al. Evidence that the two C1q binding membrane proteins, gC1q-R and cC1q-R, associate to form a complex. J Immunol 1997;159:1429–36.
35. Kolev M, Markiewski MM. Targeting complement-mediated immunoregulation for cancer immunotherapy. Semin Immunol 2018;37:85–97.
36. Bonavita E, Gentile S, Rubino M, Maina V, Papait R, Kunderfranco P, et al. PTX3 is an extrinsic oncosuppressor regulating complement-dependent inflammation in cancer. Cell 2015;160:700–14.
37. de Jong RN, Beurskens FJ, Verploegen S, Strumane K, van Kampen MD, Voorhorst M, et al. A novel platform for the potentiation of therapeutic antibodies based on antigen-dependent formation of IgG hexamers at the cell surface. PLoS Biol 2016;14:e1002344.
38. Agostinis C, Bulla R, Tripodo C, Gismondi A, Stabile H, Bossi F, et al. An alternative role of C1q in cell migration and tissue remodeling: contribution to trophoblast invasion and placental development. J Immunol 2010; 185:4420–9.
39. Bossi F, Tripodo C, Rizzi L, Bulla R, Agostinis C, Guarnotta C, et al. C1q as a unique player in angiogenesis with therapeutic implication in wound healing. Proc Natl Acad Sci U S A 2014;111:4209–14.
40. de Visser KE, Korets LV, Coussens LM. De novo carcinogenesis promoted by chronic inflammation is B lymphocyte dependent. Cancer Cell 2005;7: 411–23.
41. Diebolder CA, Beurskens FJ, de Jong RN, Koning RI, Strumane K, Lindorfer MA, et al. Complement is activated by IgG hexamers assembled at the cell surface. Science 2014;343:1260–3.
42. Braig D, Nero TL, Koch HG, Kaiser B, Wang X, Thiele JR, et al. Transitional changes in the CRP structure lead to the exposure of proinflammatory binding sites. Nat Commun 2017;8:14188.
43. Nauta AJ, Bottazzi B, Mantovani A, Salvatori G, Kishore U, Schwaeble WJ, et al. Biochemical and functional characterization of the interaction between pentraxin 3 and C1q. Eur J Immunol 2003;33:465–73.
44. Roumenina LT, Ruseva MM, Zlatarova A, Ghai R, Kolev M, Olova N, et al. Interaction of C1q with IgG1, C-reactive protein and pentraxin 3: mutational studies using recombinant globular head modules of human C1q A, B, and C chains. Biochemistry 2006;45:4093–104.
45. Agostinis C, Vidergar R, Belmonte B, Mangogna A, Amadio L, Geri P, et al. Complement protein C1q binds to hyaluronic acid in the malignant pleural mesothelioma microenvironment and promotes tumor growth. Front Immunol 2017;8:1559.
46. Ajona D, Okroj M, Pajares MJ, Agorreta J, Lozano MD, Zulueta JJ, et al. Complement C4d-specific antibodies for the diagnosis of lung cancer. Oncotarget 2018;9:6346–55.
47. Ajona D, Pajares MJ, Corrales L, Perez-Gracia JL, Agorreta J, Lozano MD, et al. Investigation of complement activation product c4d as a diagnostic and prognostic biomarker for lung cancer. J Natl Cancer Inst 2013;105: 1385–93.
48. Xi W, Liu L, Wang J, Xia Y, Bai Q, Long Q, et al. High level of anaphylatoxin C5a predicts poor clinical outcome in patients with clear cell renal cell carcinoma. Sci Rep 2016;6:29177.
49. Xi W, Liu L, Wang J, Xia Y, Bai Q, Xiong Y, et al. Enrichment of C5a-C5aR axis predicts poor postoperative prognosis of patients with clear cell renal cell carcinoma. Oncotarget 2016;7:80925–34.
50. Zafar GI, Grimm EA, Wei W, Johnson MM, Ellerhorst JA. Genetic deficiency of complement isoforms C4A or C4B predicts improved survival of metastatic renal cell carcinoma. J Urol 2009;181:1028–34.